Isostructural chiral metal-organic frameworks with metal-regulated performances for electrochemical enantiomeric recognition of tyrosine and tryptophan

Ran An, Qiu-Yan Hu, Liu-Yang Song, Xu Zhang, Rui-Xuan Li, En-Qing Gao* and Qi Yue*

School of Chemistry and Molecular Engineering, Shanghai Key Laboratory of Green Chemistry and Chemical Processes, East China Normal University, Shanghai 200241, P.R. China

Keywords: metal-organic framework, homochirality, electrochemistry, enantioselective recognition, tyrosine, tryptophan.

Supplementary information for:

Experimental section

Figures

Fig. S9. (a) DPVs of L-Trp and D-Trp with different concentrations on Co-TBLeuBpa@NF/GCE in 0.1 M PBS (pH = 7.0). (b) The linear relationship between peak current intensities and logarithmic values of different concentrations of Trp enantiomers on Co-TBLeuBpa@NF/GCE (the standard deviations of three measurements are shown for each concentration).

Fig. S10. (a) DPVs of Trp containing different ratios of L-Trp (0, 20, 40, 60, 80 and 100 %) on Co-TBLeuBpa@NF/GCE in 0.1 M PBS (pH = 7.0). (b) The relationship between peak current intensity and different L-Trp % in the racemic mixture of Trp (the standard deviations of three measurements are shown for each ratio).

Fig. S11. PXRD patterns of (a) **Cu-TBLeuBpa** and (b) **Co-TBLeuBpa** with simulated (black), synthesized (red) and immersed in the 1.0 mM L-Tyr (0.1 M PBS, pH = 10), 1.0 mM L-Tyr (0.1 M PBS, pH = 7), 1.0 mM L-Trp (0.1 M PBS, pH = 7.0).

Fig. S12. DPVs of (a) Tyr (1.0 mM) and (b) Trp (1.0 mM) enantiomers at H_2TBLeu@NF/GCE and Cu-TBLeuBpa@NF/GCE in 0.1 M PBS (pH = 7.0).

Fig. S13. The UV absorption spectra of bpea, H_2TBLeu, **Cu-TBLeuBpa**, L-Phe, bpea@L-Phe, H_2TBLeu@L-Phe, and Cu-TBLeuBpa@L-Phe.

Fig. S14. The UV absorption spectra of **Cu-TBLeuBpa**, H_2TBLeu, bpea, Phenol, Cu-TBLeuBpa@Phenol, H_2TBLeu@Phenol and bpea@Phenol.

Fig. S15. DPVs of L- and D-Tyr (1.0 mM) enantiomers at Cu-TBLeuBpa@NF/GCE in the pH range of 6.0 – 11.0.

Fig. S16. (a) DPVs of L-Tyr and D-Tyr with different concentrations on Cu-TBLeuBpa@NF/GCE in 0.1 M PBS (pH = 10.0). (b) Linear relationship between peak current intensities and logarithmic values of different concentrations of Tyr isomers on Cu-TBLeuBpa@NF/GCE (the standard deviations of three measurements are shown for each concentration).

Fig. S17. The UV absorption spectra of L-Trp, Indole, L-Ala, **Cu/Co-TBLeuBpa**, Cu/Co-TBLeuBpa@L-Trp, Cu/Co-TBLeuBpa@Indole, and Cu/Co-TBLeuBpa@L-Ala.

Fig. S18. The UV absorption spectra of bpea, H_2TBLeu, **Cu/Co-TBLeuBpa**, L-Trp, bpea@L-Trp, H_2TBLeu@L-Trp, and Cu/Co-TBLeuBpa@L-Trp.

Fig. S19. CD spectra of **Cu-TBLeuBpa**.

Fig. S20. Photograph of colloidal solution of (a) **Cu-TBLeuBpa** and (b) **Co-TBLeuBpa**.

TABLES

Table S1. Comparison of the performance of **Cu-TBLeuBpa** and the other chiral sensors for the electrochemical recognition of Tyr enantiomers.

Table S2. Crystallographic data and structure refinement for **Cu-TBLeuBpa** and **Co-TBLeuBpa**.

Table S3. Selected bond lengths and angles of **Cu-TBLeuBpa**.

Table S4. Selected bond lengths and angles of **Co-TBLeuBpa**.

Experimental Section

1 Reagents and apparatus

All reagents are analytical grade, obtained commercially and used directly without further purification. Cu $(NO_3)_2 \cdot 3H_2O$, Co $(NO_3)_2 \cdot 6H_2O$, bpea, DMF, L/D-Tyr, DL-Tyr, L/D-Trp, DL-Trp, L/D-Ala, L/D-Phe, L/D-His, indole and phenol were purchased from Shanghai Titan Technology Co., Ltd (Shanghai, China). Perfluorosulfonic acid polytetrafluoroethylene copolymer (Nafion D520, 5% w/w solution) (NF) was purchased from Alfa Aesar (China) Chemical Co., Ltd (Shanghai, China). All aqueous solutions were prepared using deionized water.

The powder X-ray diffraction data of crystals were collected by the Bruker D8 ADVANCE X-ray diffractometer. The wettability measurement was performed by the water contact angle measuring instrument (DSA-X type, KRUSS). The UV visible spectra were measured by the SHIMADZU UV-2600 spectrophotometer. The CD spectra were measured by JASCO J-1500-150 spectrophotometer.

Electrochemical behaviors including electrochemical impedance spectroscopy (EIS), cyclic voltammetry (CV), and differential pulse voltammetry (DPV) were collected through a 660E electrochemical workstation (Chenhua Instrument Shanghai Co., Ltd., China). A traditional three electrode system was used in the electrochemical analysis and included a glassy carbon electrode (GCE) (ϕ 3 mm) as the working electrode, Ag/AgCl (saturated KCl solution) as the reference electrode, platinum wire as the counter electrode. The working electrolyte were phosphate buffer solutions (0.1 M PBS, pH = 7.0 and pH = 10.0). All potentials were referenced relative to the saturated Ag/AgCl reference potential.

2 X-ray crystallography

Single crystal X-ray diffraction analysis was performed using a Braker APEX-II CCD diffractometer, with a graphite mono chromide Cu-Kα (λ = 1.54178 Å) as the radiation source, at 173 K. The crystal structures were solved by the direct method and refined by the full-matrix least-squares method on F^2 using SHELXTL-2013 program. All nonhydrogen atoms were anisotropic refined. The hydrogen atoms of coordinated water molecules were found in the different Fourier maps, while other hydrogen atoms were located at the calculated positions. The crystallography data and structural refinement of **Cu-TBLeuBpa** and **Co-TBLeuBpa** are

shown in Table S2. The selected bond lengths and angles for **Cu-TBLeuBpa** and **Co-TBLeuBpa** are listed in Table S3 and S4.

3 Synthesis of **Cu-TBLeuBpa**

$Cu(NO_3)_2 \cdot 3H_2O$ (0.03 mmoL, 0.0072 g), H_2TBLeu (0.03 mmoL, 0.0118 g), bpea (0.03 mmoL, 0.0055 g) were added to a 23 mL reactor lined with polytetrafluoroethylene containing 2 mL DMF, 6 mL H_2O and 0.5 mL HNO_3 (0.14 mM). After stirring for 40 mins, the mixed solution was put into a baking oven and reacted at 70 ^oC for 48 hrs, and cooled to room temperature. Blue prismatic crystals were collected (based on H_2TBLeu with a yield of 45 %).

4 Synthesis of **Co-TBLeuBpa**

The preparation method of **Co-TBLeuBpa** was similar to **Cu-TBLeuBpa**. Under other invariable conditions, $Co(NO_3)_2 \cdot 6H_2O$ (0.03 mmoL, 0.0087 g) replaced $Cu(NO_3)_2 \cdot 3H_2O$, 1 mL DMF and 2 mL H_2O replaced 2 mL DMF and 6 mL H_2O. The obtained solution was sealed in a 23 mL reactor at 90 ^oC for 48 hrs. Pink prismatic crystals were collected (based on H_2TBLeu with a yield of 30 %).

5 Construction of electrochemical chiral sensors

5.1. Preparation of bare GCE.

The bare glassy carbon electrode (GCE, ϕ 3 mm) was polished on suede covered with 0.05 μm Al_2O_3 suspension for several mins and sonicated with ethanol and distilled water for 5 mins to remove impurities on the surface of the electrode. After drying in a nitrogen gas flow, a usable bare GCE electrode was obtained.

5.2. Preparation of different modified GCEs.

1 mg powdered sample of **Cu-TBLeuBpa** and **Co-TBLeuBpa** were uniformly dispersed in 0.1 mL newly prepared Nafion aqueous solution (10 μL Nafion D520 dissolved in 90 μL H_2O) by the ultrasonic treatment to obtain the stable colloidal solutions of Cu-TBLeuBpa@NF and Co-TBLeuBpa@NF, respectively. And then, 2.5 μL colloidal solutions were dropped onto the surface of freshly prepared bare GCE and dried in a nitrogen flow to get successfully Cu-TBLeuBpa@NF/GCE and Co-TBLeuBpa@NF/GCE, respectively. To carry out the control experiments, the H_2TBLeu@NF/GCE sensor was prepared by the same procedure. Nafion D520 (NF) as the binder to prevent the MOFs falling off from the bare GCE during electrochemical testing.

6 Electrochemical performance characterization of the Cu-TBLeuBpa@NF/GCE and Co-TBLeuBpa@NF/GCE sensors

The cyclic voltammetry (CV) and electrochemical impedance spectroscopy (EIS) of bare GCE, Cu-TBLeuBpa@NF/GCE and Co-TBLeuBpa@NF/GCE were measured in a 5.0 mM $[Fe(CN)_6]^{4-/3-}$ electrolyte solution containing 0.1 M KCl. The EIS signals were collected in the scanning frequency range of 10^6 − 0.01 Hz, and the CV signals were collected in the potential range of -0.6 − 0.8 V.

7 Enantioselective recognition of amino acid enantiomers by the Cu-TBLeuBpa@NF/GCE and Co-TBLeuBpa@NF/GCE sensors

7.1 Enantioselective recognition of amino acid enantiomers

The differential pulse voltammograms (DPVs) of amino acid enantiomers at the Cu-TBLeuBpa@NF/GCE and Co-TBLeuBpa@NF/GCE sensors were collected in 10 mL 0.1 M PBS containing 1.0 mM various enantiomers (including L/D-Tyr, L/D-Trp, L/D-Phe, L/D-His and L/D-Ala,) to probe the chiral recognition abilities of sensors. The enantioselective recognition efficiency of the modified electrodes was evaluated by the peak current ratio (I_L/I_D) and the difference in peak potential ($\Delta E_p = E_L - E_D$).

The DPV responses to L/D-Tyr and L/D-Trp with the concentration range from 10^{-7} to 10^{-3} M in 10 mL 0.1 M PBS using the Cu-TBLeuBpa@NF/GCE and Co-TBLeuBpa@NF/GCE sensors were monitored to determine the limit of detection of L/D-Tyr and L/D-Trp.

7.2 Quantitative determination of Tyr and Trp enantiomers in racemic mixtures.

The DPV profiles of Tyr and Trp enantiomers were collected on Cu-TBLeuBpa@NF/GCE and Co-TBLeuBpa@NF/GCE in 10 mL 0.1 M PBS containing 1.0 mM L-enantiomers. The relative contents of L-enantiomers were 0 %, 20 %, 40 %, 60 %, 80 % and 100 %, respectively.

7.3 Quantitative determination of Tyr and Trp enantiomers by Cu-TBLeuBpa@NF/GCE in human urine

Human urine samples were provided by the first author (a healthy female postgraduate). 10 mL urine samples were centrifuged at 6000 r·min^{-1} for 15 mins. The supernatant was passed through 0.22 μM aqueous phase filtration membrane, afterwards, 5 mL filtrate was diluted to 100 mL with 0.1 M PBS (pH = 7.0) for the determination of DPV signals.

The L-Tyr and L-Trp standard solution with concentrations of 1, 10, 20 and 40 μM were

added to 10 mL urine samples (spiked three times for every concentration), respectively. DPV curves of L-Tyr and L-Trp in urine samples were collected by using Cu-TBLeuBpa@NF/GCE. The recovery rates and the relative standard deviation of samples are shown in Table 1.

8 Experiment procedure of recognition mechanism

8.1 UV-visible spectra

6.4 mg fully ground powder sample of **Cu-TBLeuBpa** was uniformly dispersed into 100 mL deionized water by ultrasonication for 40 mins. A stable colloidal solution was obtained as the crystal stock solution. In the experiment of exploring the interaction between chiral frameworks and guest molecules, the 0.5 mL 1.0 mM L-Tyr, L-Trp, L-Phe, L-Ala, phenol and indole aqueous solutions were added to 2 mL **Cu-TBLeuBpa** stock solution, respectively. The resulted mixture solutions were measured after 40 mins of ultrasonic treatment for the analysis of the UV-visible spectra. In order to ensure comparability, 0.5 mL deionized water was added to the 2 mL stock solution of **Cu-TBLeuBpa** and 2 mL deionized water is added to the 0.5 mL aqueous solution of above guest molecules, respectively. The same treatment method was also employed to probe the interaction between the **Co-TBLeuBpa** framework and guest molecules.

8.2 CD spectra

The CD spectra of 2 mL 0.5 mM **Cu-TBLeuBpa** stock solution, L-Tyr, D-Tyr, and DL-Tyr aqueous solutions were respectively measured using H_2O as the background. The 4 mL 0.5 mM **Cu-TBLeuBpa** stock solution was added to 1 mL 0.5 mM DL-Tyr, then mixture solution was sonicated for 30 mins and centrifuged. The 2 mL supernatant labeled as DL-Tyr* was taken out for monitoring corresponding CD spectra by the **Cu-TBLeuBpa** stock solution as the background.

8.3 Wettability measurements

The 3 mg fully ground powder sample of **Cu-TBLeuBpa** was dispersed into 10 mL 1.0 mM L-Tyr, D-Tyr and H_2O by the ultrasound treatment for 60 mins, respectively. The obtained corresponding mixture solutions were centrifuged to extract the 30 μL supernatant, which was spin coated on the glass slides by a film plating machine (with a speed of 2000 $r \cdot s^{-1}$ and a time of 20 s). The glass slides were dried under infrared light for 5 mins for the wettability testing.

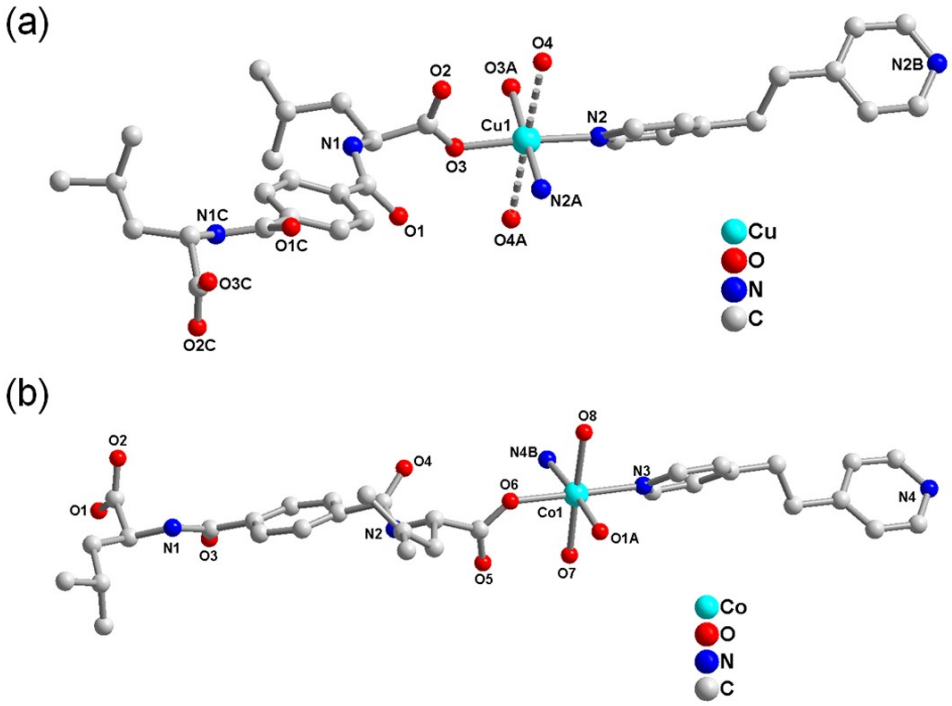

Fig. S1. (a) Coordination environment of the Cu(II) ion in **Cu-TBLeuBpa** (Symmetry codes: A = 1-x, y, 1-z; B = 2-x, 2-y, 0.75-z). (b) Coordination environment of the Co(II) ion in **Co-TBLeuBpa**. (Symmetry codes: A = 1-x, y, z; B = x, 2-y, -0.25+z). All hydrogen atoms have been omitted for clarity.

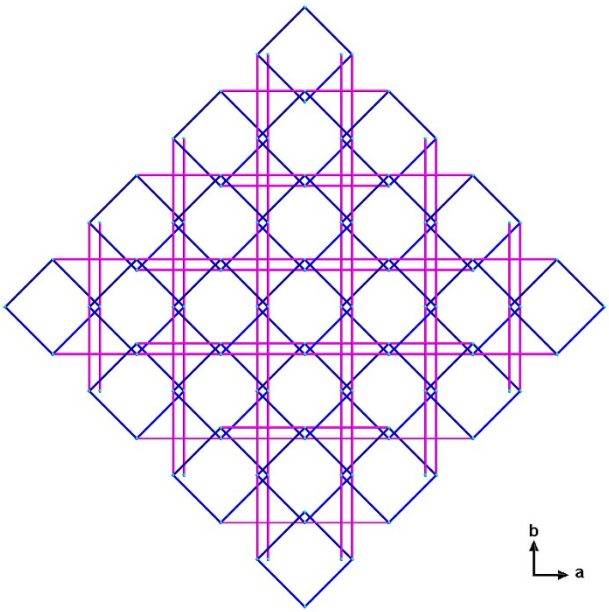

Fig. S2. 3D topological framework of **Cu-TBLeuBpa** viewed along the *c*-axis.

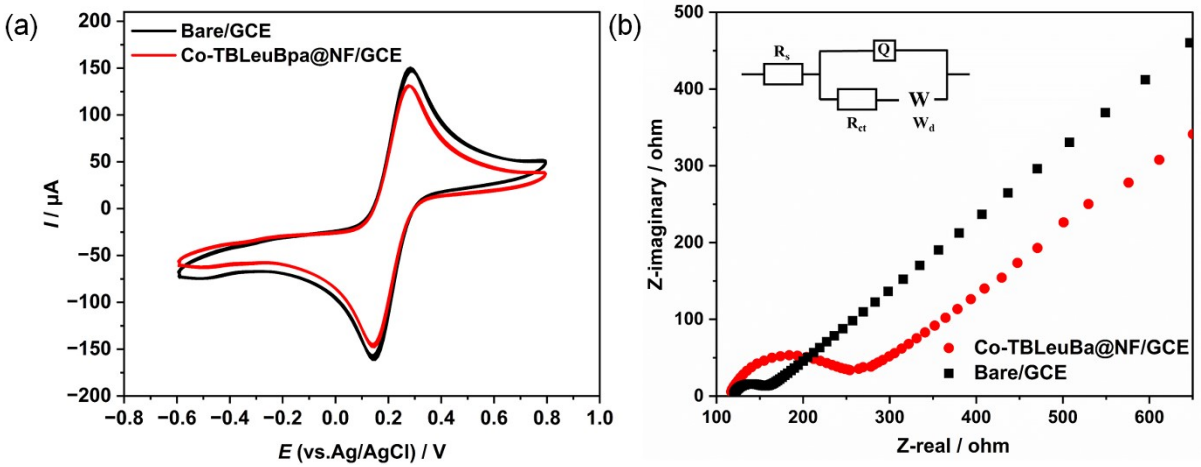

Fig. S3. (a) CVs of bare GCE and Co-TBLeuBpa@NF/GCE. (b) EIS of bare GCE and Co-TBLeuBpa@NF/GCE. Tests were carried out in a 5.0 mM $[Fe(CN)_6]^{4-/3-}$ solution containing 0.1 M KCl. Inset is the corresponding equivalent circuit, where R_s is the solution resistance, R_{ct} is the interfacial charge transfer resistance, W_d is the Warburg resistance, and Q represents the constant phase elements (CPEs).

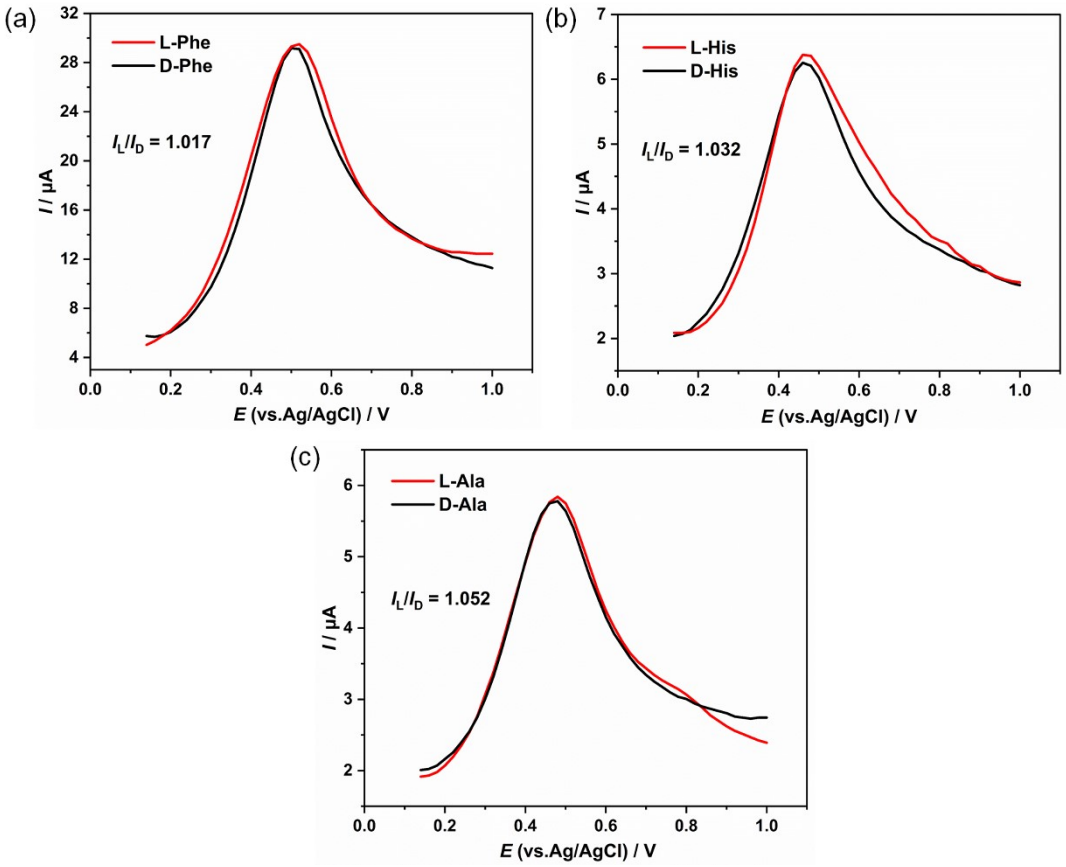

Fig. S4. DPVs of (a) Phe, (b) His and (c) Ala enantiomers (1.0 mM) at Cu-TBLeuBpa@NF/GCE in 0.1 M PBS (pH = 7.0).

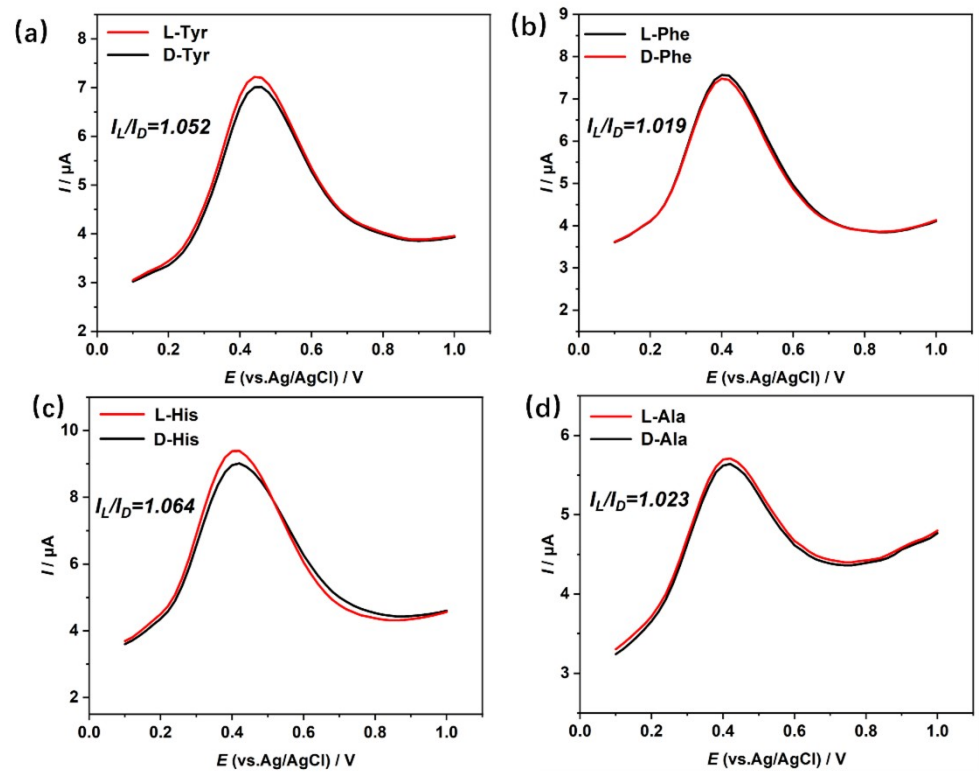

Fig. S5. DPVs of (a) Tyr, (b) Phe, (c) His and (d) Ala enantiomers (1.0 mM) at Co-TBLeuBpa@NF/GCE in 0.1 M PBS (pH = 7.0).

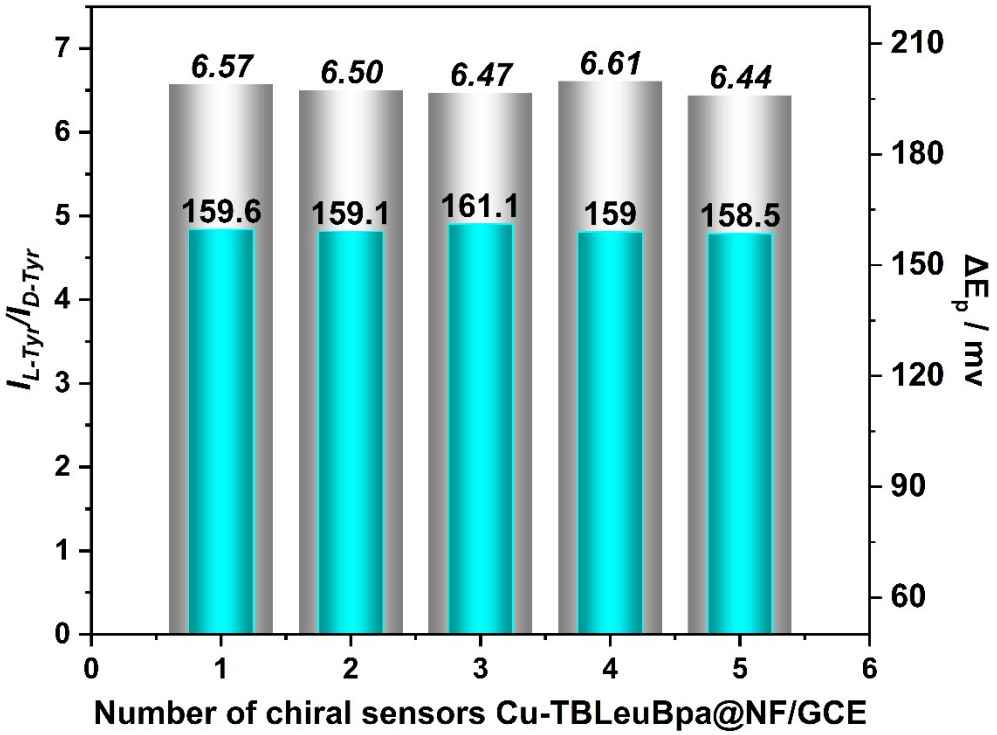

Fig. S6. Peak current ratio and potential difference for Tyr enantiomers with five independently prepared Cu-TBLeuBpa@NF/GCE sensors in 0.1 M PBS (pH = 7.0).

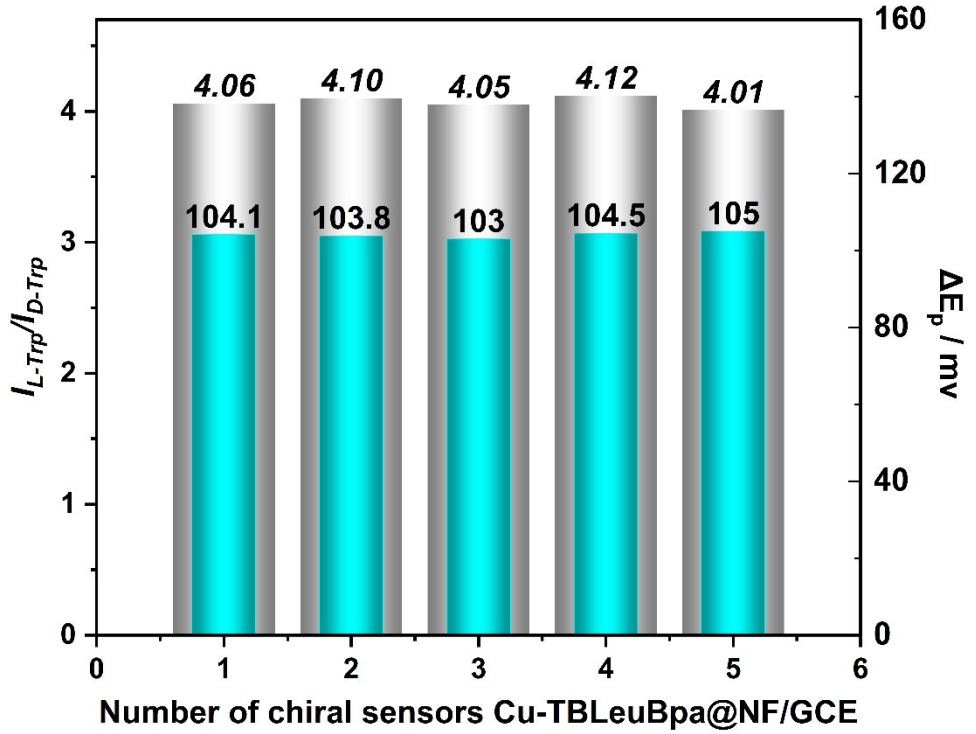

Fig. S7. Peak current ratio and potential difference for Trp enantiomers with five independently prepared Cu-TBLeuBpa@NF/GCE sensors in 0.1 M PBS (pH = 7.0).

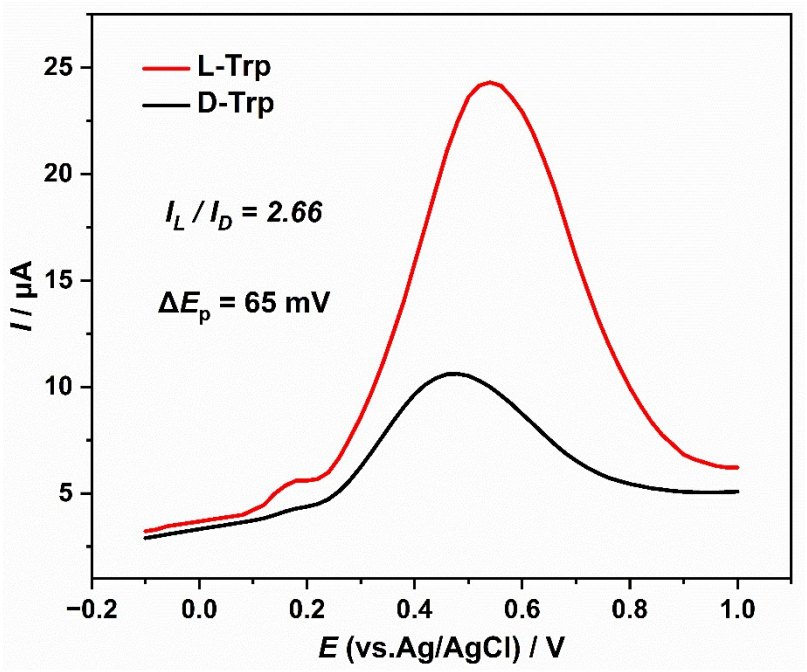

Fig. S8. DPVs of L- and D-Trp (1.0 mM) at Co-TBLeuBpa@NF/GCE in 0.1 M PBS (pH = 7.0).

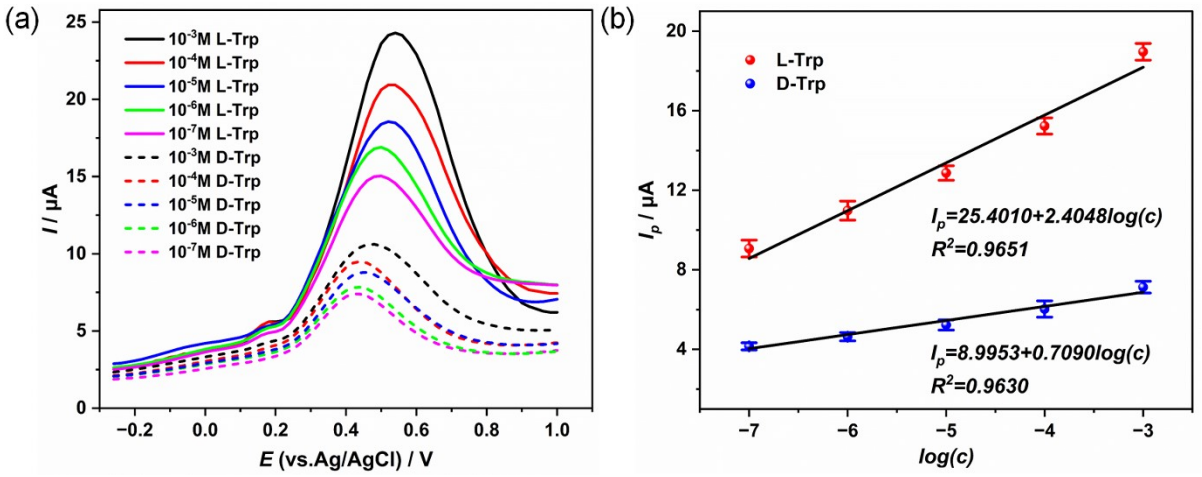

Fig. S9. (a) DPVs of L-Trp and D-Trp with different concentrations on Co-TBLeuBpa@NF/GCE in 0.1 M PBS (pH = 7.0). (b) The linear relationship between peak current intensities and logarithmic values of different concentrations of Trp enantiomers on Co-TBLeuBpa@NF/GCE (the standard deviations of three measurements are shown for each concentration).

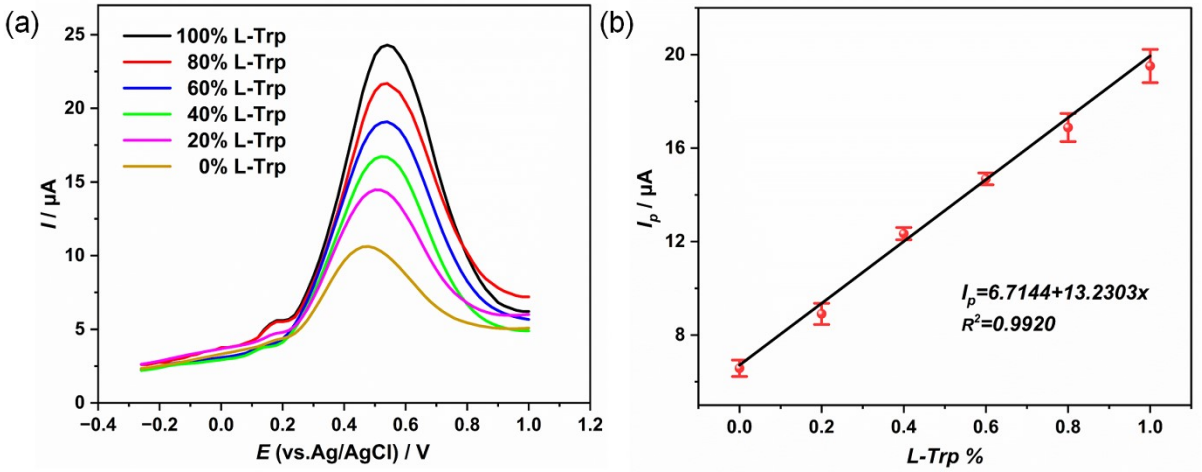

Fig. S10. (a) DPVs of Trp enantiomers containing different ratios of L-Trp (0, 20, 40, 60, 80 and 100 %) on Co-TBLeuBpa@NF/GCE in 0.1 M PBS (pH = 7.0). (b) The relationship between peak current intensity and different L-Trp % in the racemic mixture of Trp enantiomers (the standard deviations of three measurements are shown for each ratio).

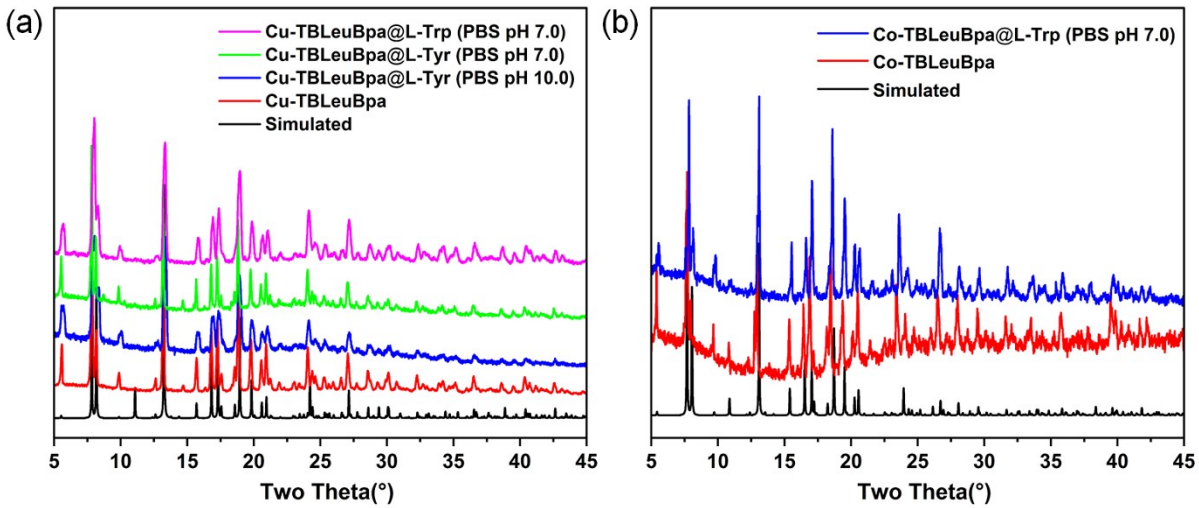

Fig. S11. PXRD patterns of (a) **Cu-TBLeuBpa** and (b) **Co-TBLeuBpa** with simulated (black), synthesized (red) and immersed in the 1.0 mM L-Tyr (0.1 M PBS, pH = 10.0), 1.0 mM L-Tyr (0.1 M PBS, pH = 7.0), 1.0 mM L-Trp (0.1 M PBS, pH = 7.0).

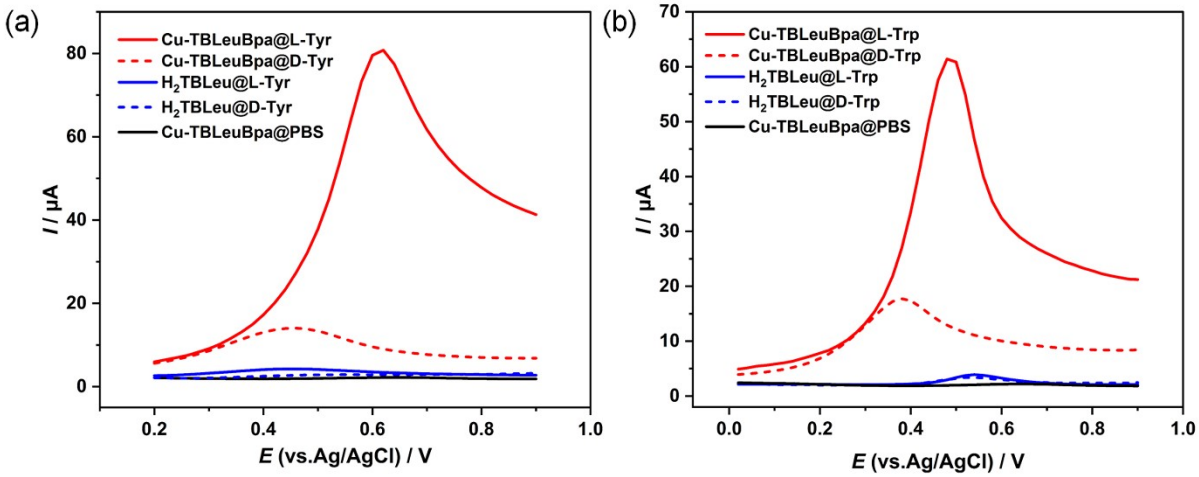

Fig. S12. DPVs of (a) Tyr (1.0 mM) and (b) Trp (1.0 mM) enantiomers at H_2TBLeu@NF/GCE and Cu-TBLeuBpa@NF/GCE in 0.1 M PBS (pH = 7.0).

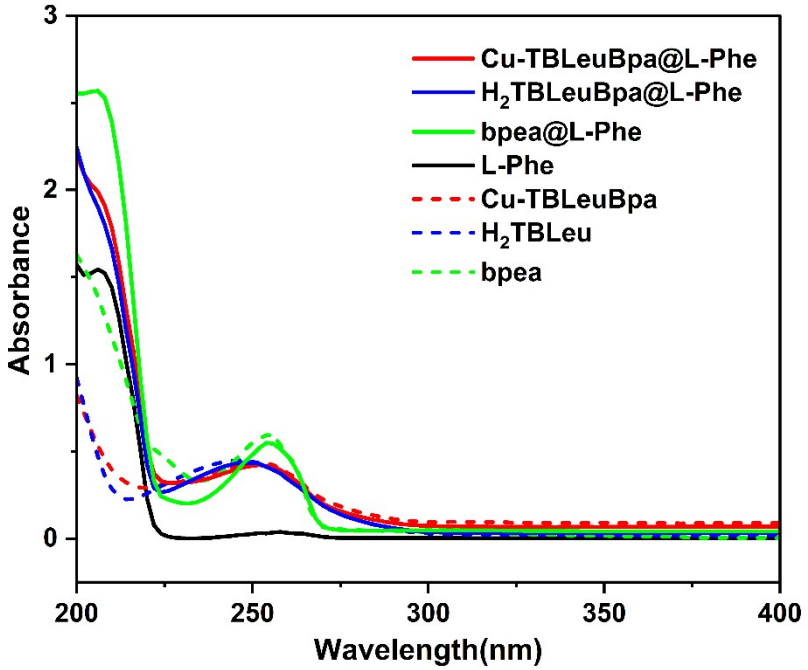

Fig. S13. The UV absorption spectra of bpea, H_2TBLeu, **Cu-TBLeuBpa**, L-Phe, bpea@L-Phe, H_2TBLeu@L-Phe, and Cu-TBLeuBpa@L-Phe.

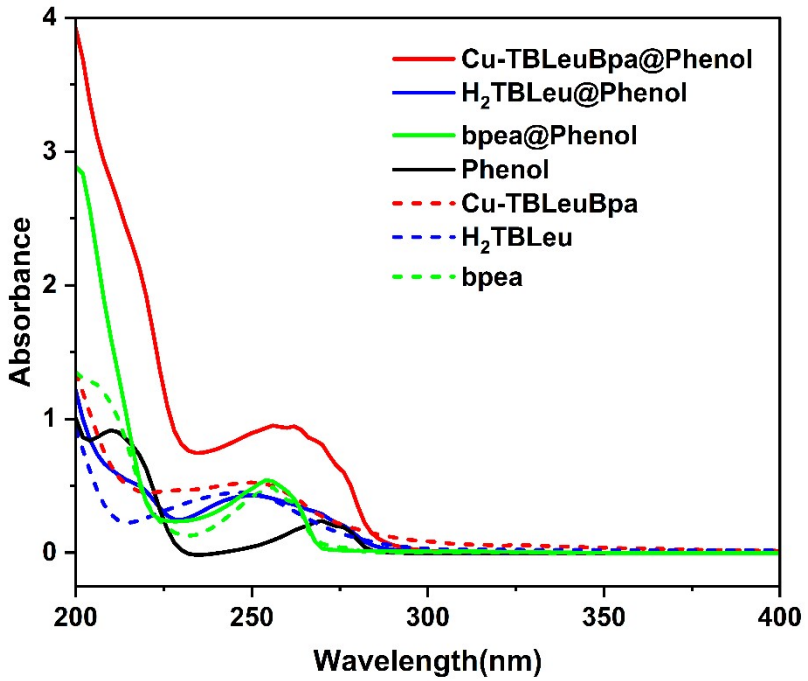

Fig. S14. The UV absorption spectra of **Cu-TBLeuBpa**, H_2TBLeu, bpea, Phenol, Cu-TBLeuBpa@ Phenol, H_2TBLeu@Phenol and bpea@Phenol.

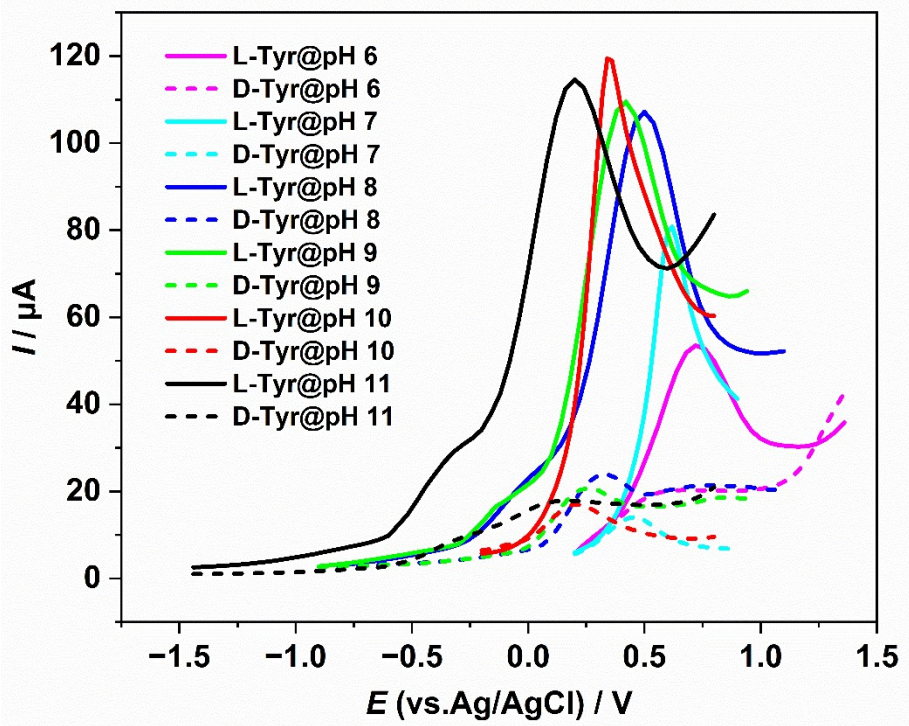

Fig. S15. DPVs of L- and D-Tyr (1.0 mM) enantiomers at Cu-TBLeuBpa@NF/GCE in the pH range of 6.0 – 11.0.

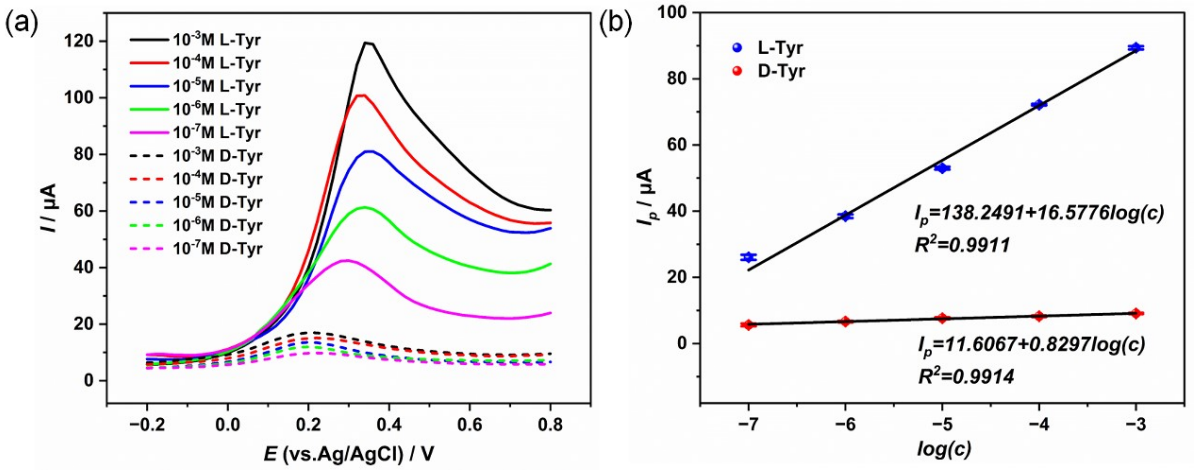

Fig. S16. (a) DPVs of L-Tyr and D-Tyr with different concentrations on Cu-TBLeuBpa@NF/GCE in 0.1 M PBS (pH = 10.0). (b) Linear relationship between peak current intensities and logarithmic values of different concentrations of Tyr isomers on Cu-TBLeuBpa@NF/GCE (the standard deviations of three measurements are shown for each concentration).

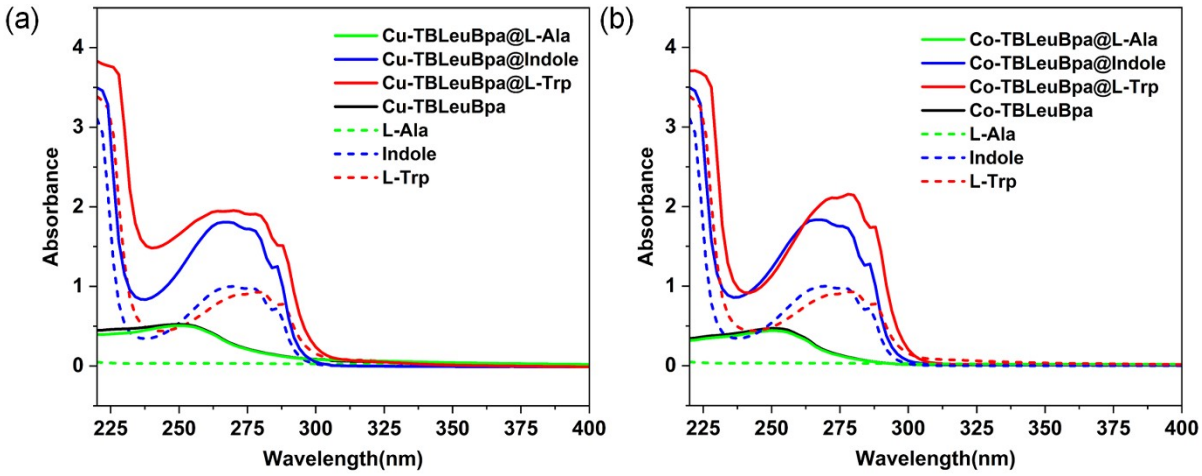

Fig. S17. The UV absorption spectra of L-Trp, Indole, L-Ala, **Cu/Co-TBLeuBpa**, Cu/Co-TBLeuBpa@L-Trp, Cu/Co-TBLeuBpa@Indole, and Cu/Co-TBLeuBpa@L-Ala.

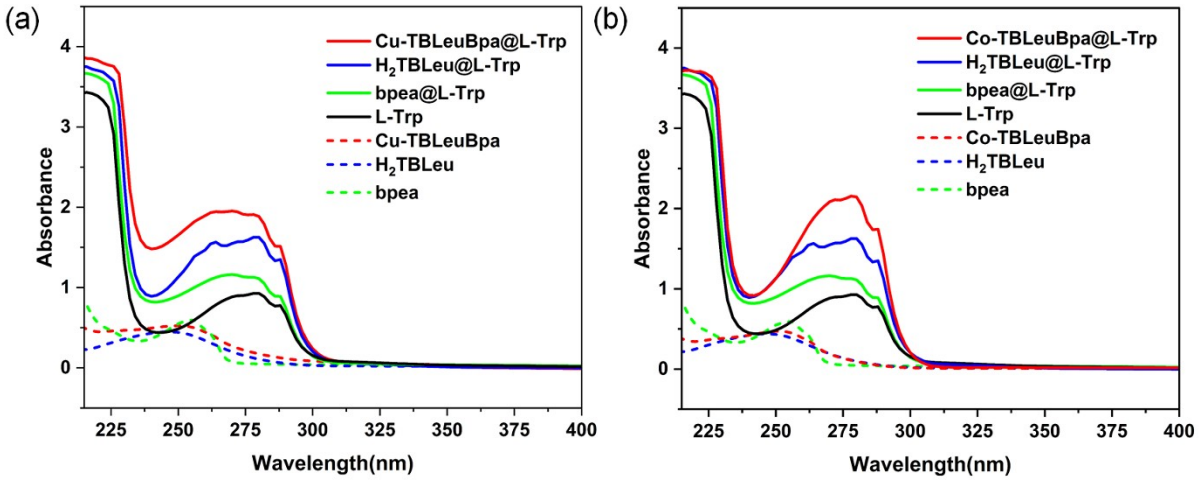

Fig. S18. The UV absorption spectra of bpea, H_2TBLeu, **Cu/Co-TBLeuBpa**, L-Trp, bpea@L-Trp, H_2TBLeu@L-Trp, and Cu/Co-TBLeuBpa@L-Trp.

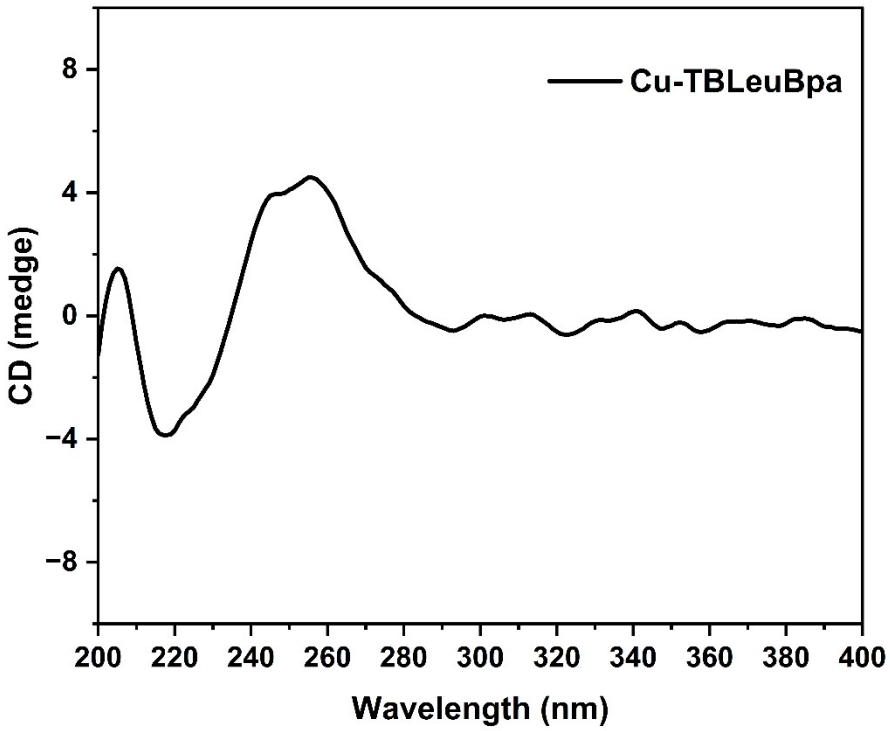

Fig. S19. CD spectra of **Cu-TBLeuBpa**.

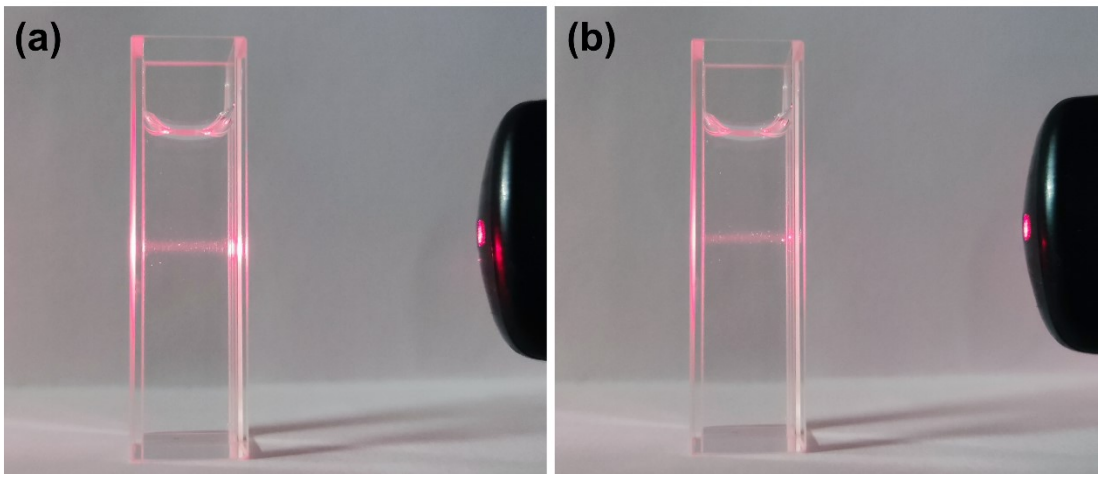

Fig. S20. Photograph of colloidal solution of (a) **Cu-TBLeuBpa** and (b) **Co-TBLeuBpa**.

Table S1. Comparison of the performance of **Cu-TBLeuBpa** and the other chiral sensors for the electrochemical recognition of Tyr enantiomers.

Electrode	Method	Recognition efficiency (I_L/I_D)	ΔE_p (mV)	Linear range (μM)	LOD of L-Tyr (D-Tyr) (nM)	Ref.
D-DHCNT@PPy@AuNPs@D-Cys/GCE	DPV	14.2	28	0-30	12 (6)	[5]
L-DHCNT@PPy@AuNPs@L-Cys/GCE	DPV	5.2	27.6	0-30	46 (68)	[5]
CS-Cu2-α-CD/GCE	DPV	3.83	112	-	-	[15]
helicoid Au NPs/GCE	DPV	5.8	-	-	-	[19]
β-CD/AgNPs/GCE	DPV	3.43	-	-	-	[20]
MPC-SCD/GCE	DPV	1.12 μA (I_L-I_D)	-	1-500	200 (260)	[22]
L-CNT@PPy@Pt NPs@β-CD/SPE	DPV	2.62 (I_D/I_L)	26.09	3-30	0.24 (0.00129)	[23]
D-CNT@PPy@Pt NPs@β-CD/SPE	DPV	8.79	44	3-30	0.107 (1.495)	[23]
3D-rGO/Pd@Au/CM-β-CD	DPV	2.12	-	0.8-130	52 (96)	[24]
GSH-Cu/Pt/GCE	DPV	5.11	104	-	-	[29]
rGO-CHMF/GCE	DPV	1.58	70	0.1-10	78 (83)	[30]
GC/(CNT+ILC/CW)/GCE	DPV	3.09	50	0.01-60	1.42 (9.36)	[34]
Cu-TBLeuBpa@NF/GCE	DPV	6.57 (pH 7.0)	160	0.1-1000	2.9 (19.8)	This work
		9.83 (pH 10.0)	150	0.1-1000	1.8 (35.8)	This work

Table S2. Crystallographic data and structure refinement for **Cu-TBLeuBpa** and **Co-TBLeuBpa**.

Compound	**Cu-TBLeuBpa**	**Co-TBLeuBpa**
Formula	$C_{32}H_{42}CuN_4O_8$	$C_{32}H_{42}CoN_4O_8$
Molecular	674.25	669.63
Crystal system	Tetragonal	Tetragonal
space group	$P4_322$	$P4_3$
a (Å)	15.95510(10)	16.2614(3)
b (Å)	15.95510(10)	16.2614(3)
c (Å)	14.6859(2)	14.8555(6)
α (°)	90	90
β (°)	90	90
γ (°)	90	90
V(Å^3)	3738.52(7)	3928.3(2)
Z	4	4
ρ_{calcd}(Mg cm^{-3})	1.198	1.132
μ(CuK$_\alpha$)(mm^{-1})	1.230	3.811
F(000)	1420	1412
Reflections collected/ unique	40089 / 3341	43540 / 6072
R_{int}	0.0743	0.1086
Data/ restraints/ parameters	3341 / 232 / 212	6072 / 195 / 400
Goodness-of-fit on F^2	1.050	1.070
R_1/wR_2[$I>_2\sigma(I)$]	0.0511, 0.1405	0.0745, 0.2019
R_1/wR$_2$[all data]	0.0531, 0.1434	0.0836, 0.2084
Largest residues (e A^{-3})	0.795, -0.591	0.443, -0.655
Absolute structure parameter	0.008(13)	0.066(9)

Table S3. Selected bond lengths and angles of **Cu-TBLeuBpa**.

Bond	Distance
Cu(1)-O(3)	1.941(3)
Cu(1)-O(4)	2.641(3)
Cu(1)-N(2)	2.002(4)
Moiety	**Angle**
O(3)#1-Cu(1)-O(3)	88.59(19)
O(3)#1-Cu(1)-N(2)	90.58(14)
O(3)-Cu(1)-N(2)	174.39(15)
O(3)#1-Cu(1)-N(2)#1	174.39(15)
O(3)-Cu(1)-N(2)#1	90.58(14)
N(2)-Cu(1)-N(2)#1	90.8(2)

Symmetry transformations used to generate equivalent atoms:
#1 -x+1,y,-z+1 #2 -x,y,-z+1 #3 -y+2,-x+2,-z+3/4

Table S4. Selected bond lengths and angles of **Co-TBLeuBpa**.

Bond	Distance
Co(1)-O(6)	2.094(5)
Co(1)-O(1)#1	2.074(5)
Co(1)-O(7)	2.103(5)
Co(1)-N(4)#2	2.121(7)
Co(1)-O(8)	2.133(5)
Co(1)-N(3)	2.138(6)
Moiety	**Angle**
O(1)#1-Co(1)-O(6)	88.8(2)
O(1)#1-Co(1)-O(7)	88.2(2)
O(6)-Co(1)-O(7)	91.1(2)
O(1)#1-Co(1)-N(4)#2	175.6(3)
O(6)-Co(1)-N(4)#2	88.2(2)
O(7)-Co(1)-N(4)#2	88.7(3)
O(1)#1-Co(1)-O(8)	91.3(2)
O(6)-Co(1)-O(8)	90.2(2)
O(7)-Co(1)-O(8)	178.6(2)
N(4)#2-Co(1)-O(8)	91.9(3)
O(1)#1-Co(1)-N(3)	90.6(2)
O(6)-Co(1)-N(3)	178.3(3)
O(7)-Co(1)-N(3)	90.4(2)
N(4)#2-Co(1)-N(3)	92.6(3)
O(8)-Co(1)-N(3)	88.3(2)

Symmetry transformations used to generate equivalent atoms:
#1 x-1, y, z #2 -y+2, x, z-1/4 #3 y, -x+2, z+1/4 #4 x+1, y, z